

Article

Mean-Line Design of a Supercritical CO₂ Micro Axial Turbine

Salma I. Salah ^{*}, Mahmoud A. Khader, Martin T. White  and Abdunaser I. Sayma

School of Mathematics, Computer Science and Engineering, City University of London, Northampton Square, London EC1V 0HB, UK; M.Khader@city.ac.uk (M.A.K.); Martin.White@city.ac.uk (M.T.W.); A.Sayma@city.ac.uk (A.I.S.)

* Correspondence: salma.salah.2@city.ac.uk

Received: 28 May 2020 ; Accepted: 27 June 2020; Published: 23 July 2020



Abstract: Supercritical carbon dioxide (sCO₂) power cycles are promising candidates for concentrated-solar power and waste-heat recovery applications, having advantages of compact turbomachinery and high cycle efficiencies at heat-source temperature in the range of 400 to 800 °C. However, for distributed-scale systems (0.1–1.0 MW) the choice of turbomachinery type is unclear. Radial turbines are known to be an effective machine for micro-scale applications. Alternatively, feasible single-stage axial turbine designs could be achieved allowing for better heat transfer control and improved bearing life. Thus, the aim of this study is to investigate the design of a single-stage 100 kW sCO₂ axial turbine through the identification of optimal turbine design parameters from both mechanical and aerodynamic performance perspectives. For this purpose, a preliminary design tool has been developed and refined by accounting for passage losses using loss models that are widely used for the design of turbomachinery operating with fluids such as air or steam. The designs were assessed for a turbine that runs at inlet conditions of 923 K, 170 bar, expansion ratio of 3 and shaft speeds of 150k, 200k and 250k RPM respectively. It was found that feasible single-stage designs could be achieved if the turbine is designed with a high loading coefficient and low flow coefficient. Moreover, a turbine with the lowest degree of reaction, over a specified range from 0 to 0.5, was found to achieve the highest efficiency and highest inlet rotor angles.

Keywords: concentrated-solar power, supercritical carbon dioxide cycle, axial turbine design, micro-scale turbomachinery design.

1. Introduction

Micro-gas turbines coupled with concentrated-solar power systems (CSP) can provide a viable solution for renewable energy generation. They have been shown to be ideally suited for small-scale standalone and off-grid applications [1]. However, micro-gas turbines experience larger losses in the system components, and hence achieve lower thermal efficiencies, compared to large-scale gas turbines. Thus, for a high thermal efficiency, in the range of 40 to 50%, the system needs to operate at high heat-source temperatures, above 600 °C. In comparison, cycles operating with supercritical carbon dioxide (sCO₂) can achieve similar thermal efficiencies at more moderate temperatures. Therefore, sCO₂ can be considered as a potential candidate for concentrated-solar power applications, particularly for stand-alone solar dish units; offering a simple layout, high-power density and compact structures [2].

Despite the promising potential of sCO₂, sCO₂ turbomachine design is still a developing field. However, turbine performance is one of the main factors that affects the cycle performance; for example, a 2% increase in turbine efficiency has been shown to result in a 1% enhancement in the thermodynamic cycle efficiency [3]. This would have a significant impact on cost reduction of the solar power system

through reduction in the size and the cost of the concentrator which typically represents over 60% of the total system cost. Therefore, several researchers have investigated advancing the state-of-the-art with regards to turbine design.

Moroz et al. [4] discussed some design aspects for a 100 MW axial sCO₂ turbine for a direct sCO₂ recompression cycle. Aerodynamic and structural analyses were performed to determine the best design configuration as a function of the number of stages, radial tip clearance and rotational speed. Holaind et al. [5] addressed the design of small radial turbomachinery with an output power ranging from 50–85 kW and an efficiency of 70%. Subsequent to that, Qi et al. [6] presented a new insight for a sCO₂ radial turbine design for a power rating ranging between 100 and 200 kW through the integration of mean-line design with a loss model where an efficiency of 78–82% has been achieved. Saeed et al. [3] developed an algorithm that allows for the design of a sCO₂ radial turbine for CSP application rated at 10 MW. During the design process, a mean-line design tool that uses an enthalpy loss model, geometry optimisation and 3D RANS simulation were performed. As a result of the geometry optimisation, an enhancement in both the efficiency and power output of 5.34% and 5.30% was achieved respectively [3]. In the same context, Zhou et al. [7] and Zhang et al. [8] proposed 300 kW and 1.5 MW radial sCO₂ turbine designs respectively. Zhang et al. [8] added a design of a 15 MW sCO₂ axial turbine to their study. They implemented CFD simulations to analyse the flow characteristics of sCO₂ turbine components. In the same year, Lv et al. [9] developed an optimisation design approach for a radial-inflow turbine using sCO₂. This was done through combining a one-dimensional design method with an optimisation algorithm for both nominal and off design performance conditions for the stage inlet temperature, rotational speed and expansion ratio. Likewise, Shi et al. [10] presented an optimal 10 MW three-stage sCO₂ axial turbine design using 3D model, optimisation methods and off design analysis. Considering the potential of sCO₂ fluid for small-scale systems, White et al. [11] presented a comparative study between various turbine architectures for a small-scale 100 kW sCO₂ Rankine cycle. Single-stage radial-inflow, single-stage axial, and two-stage axial turbines were analysed to identify the most feasible turbine designs based on the limitations of the blade height. It was found that the feasible blade height is in the range of 1.74 to 2.47 mm for a given turbine diameter of 30 mm. Furthermore, it was concluded that a low degree of reaction is preferred for single-stage turbines resulting in supersonic conditions at the rotor inlet. However, a higher degree of reaction is suitable for two-axial stage turbine leading to subsonic rotor inlet conditions.

Besides the aforementioned research work in the field of sCO₂ turbo-machines designs, a large amount of work has been conducted for micro-scale organic Rankine cycle (ORC) turbine design, using the same design methodology for novel working fluids, including refrigerants such as R134a, R1234yf and R152a. Fiaschi et al. [12] developed a design tool that included a loss model to examine the performance of a 50 kW radial turbine operating with various working fluids. The results of the study demonstrated that an efficiency ranging from 78–85% can be achieved with a highest value (85%) for R134a and lowest value (78%) for R1234yf. Casati et al. [13] developed two preliminary designs for a five-stage transonic and eight stage supersonic radial-outflow 10 kW ORC turbine. It was found that the transonic turbines outperform the supersonic turbine during the partial-load operations thus resulting in enhanced efficiency. Rahbar et al. [14] proposed a mean-line model integrated with both an optimisation algorithm and a real-gas formulation for a 15 kW radial turbine. The design model resulted in a turbine efficiency ranging from 82.4–84% with a maximum value found for R152a. Lio et al. [15] integrated both mean-line design with loss correlations, developed previously for radial gas turbines, for examining turbine size, working conditions and predicting the efficiency of radial-inflow turbine operating with R245fa. The study revealed that the turbine size has a noticeable effect on the efficiency, and thus an efficiency of 85 to 90% at high expansion ratio has been attained at an output power greater than 50 kW.

Radial turbines are known to be an effective and compact machine for small-scale applications with a power ranging from 50 kW to 5 MW, allowing for the expansion of the working fluid in one single stage [12]. Thus, the radial-inflow turbine configuration has been the main candidate for small-size

turbomachinery design in most of the aforementioned researches. Alternatively, a feasible single-stage axial turbine design could be achieved for micro-scale applications allowing for better heat transfer control, as the hot blades are far from the shaft, and subsequently prolongs the life of the bearing. In the current study, a mean-line approach is used to address the design of a single-stage 100 kW sCO₂ axial turbine design through identifying optimal turbine design parameters from both mechanical perspectives, owing to the significant axial thrust loads, high rotational speeds and high operating pressures, and aerodynamic performance perspectives. Additionally, the design tool implemented in the current study is refined by introducing Soderberg's and Ainley and Mathieson's loss correlations, which allows the loss within the rotor and stator to be estimated based on loading coefficient, tip clearance and blade geometry. The designs were evaluated at three different speeds of 150k, 200k, 250k RPM respectively, to achieve an overall turbine efficiency greater than 80% and keep low centrifugal stresses on the rotor blades, for turbine inlet conditions of 923 K, 170 bar, expansion ratio of 3. For the given inlet conditions, a single-stage design is proposed due to the low power rating and low volume ratio of the machine. The novelty in this current work lies in presenting a design of sCO₂ micro-scale single-stage axial turbine, alongside with defining the optimal turbine design parameters from both mechanical and aerodynamic performance perspectives.

This paper is structured as follows: an overview of turbine design methodology and assumptions are presented in Section 2. Axial turbine design and loss modelling is discussed in Section 3. The results and discussion are presented in Section 4, before the final conclusions are presented.

2. Turbine Design Methodology

sCO₂ condensation (transcritical) power cycles were firstly proposed by Angelino and Feher in 1968 where efficiencies up to 50 % can be achieved [16,17]. However, to achieve condensation within the cycle it is necessary to lower the temperature of the CO₂ below its critical temperature (31.1 °C). Unfortunately, achieving this within CSP plants, which are typically in dry arid regions with high solar irradiation, requires water-cooling which is usually not feasible in these sites. To overcome this issue, it has been proposed to raise the critical point of the working fluid by doping CO₂ with another fluid. For example, mixing CO₂ with various additives, such as C₃H₈, C₄H₈, C₄H₁₀, C₅H₁₀, C₅H₁₂ and C₆H₆, has been shown to increase the critical temperature to up to 60 °C [18]. Moreover, the application of sCO₂ blends in CSP plants have been previously studied [18] and have been shown to enhance efficiency of a Brayton power cycle by 3–4% compared to pure sCO₂. Therefore, sCO₂ blends have been proposed instead of pure sCO₂ to increase the critical temperature of the working fluid [19,20]. The presented design methodology has been developed as part of a preliminary study related to the Horizon 2020 SCARABEUS project [21], and thus the methodology is capable of designing turbines intended for sCO₂ blends. However, for simplicity at this stage, pure sCO₂ will be considered as the working fluid. Considering a blend merely changes the inputs into the equation of state used to predict thermodynamic properties and thus the method can be readily extended to blends without any change to the analysis. It should be noted that the turbine design is likely to be sensitive to the chosen blend, but such investigations are left for a future work.

The turbine design is part of a condensation sCO₂ cycle, as shown in Figures 1 and 2, with a net power output of 100 kW. The turbine inlet parameters are obtained from a thermodynamic cycle analysis and are selected as a compromise between cycle efficiency, component life, complexity and feasibility [11]. Accordingly, the turbine inlet temperature is limited to 650 °C. The turbine inlet pressure is limited to 17 MPa with an expansion ratio of 3 to reduce the power block weight, size and price [22]. The cycle is designed assuming a pump inlet temperature of 20 °C, pressure of 6 MPa, compressor isentropic efficiency of 70%, turbine isentropic efficiency of 80% and recuperator effectiveness of 90%. For the selected parameters, the cycle has a thermal efficiency of 32.8% with a mass-flow rate of 0.65 kg/s.

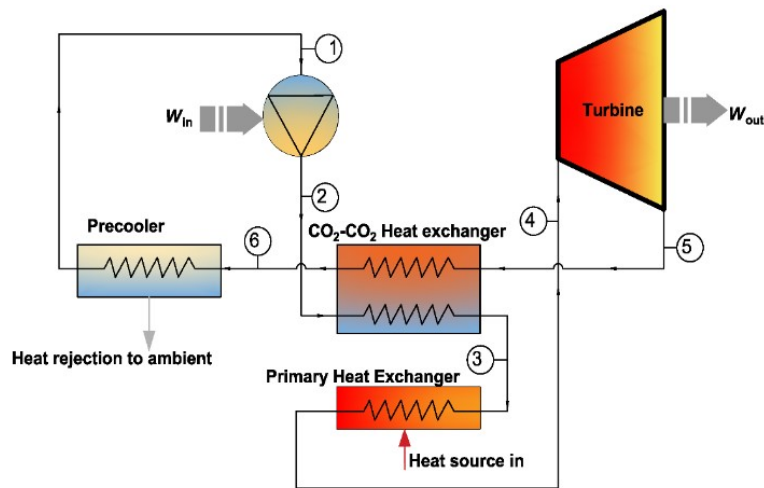


Figure 1. Cycle schematic drawing.

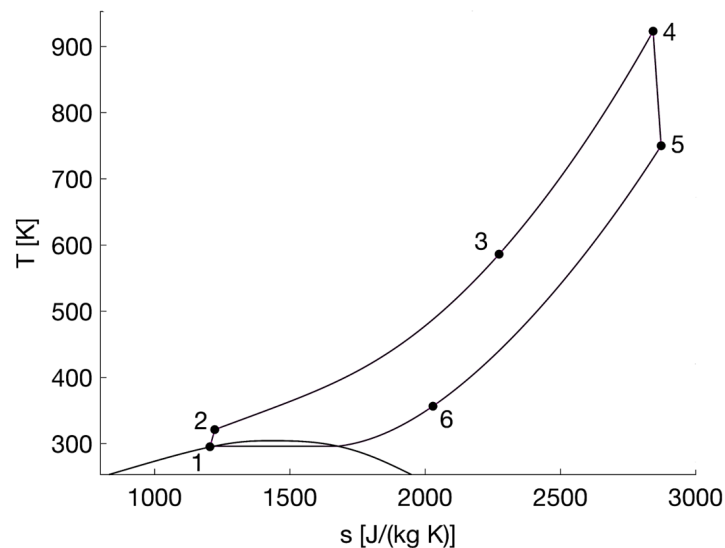


Figure 2. Entropy versus temperature (T - s diagram) for the thermodynamic cycle in Figure 1.

To design the turbine, a mean-line turbine design approach is adopted to provide a fast and accurate estimation of the turbine geometry and the expected isentropic efficiency. This has been developed in MATLAB and coupled with NIST REFPROP [23] to account for the $s\text{CO}_2$ fluid behaviour. The model is also capable of operating with Simulis, which enables novel fluid blends to be considered [24]. Within the model the steady-state mass, energy and momentum equations are solved to obtain the geometric parameters of the turbine. In this section, the turbine mean-line design is developed along with a parametric study to examine the effect of changing various design parameters on the turbine performance, at various rotational speeds, and assess blades pressure and centrifugal loads. The designs were evaluated for turbine inlet conditions of 923 K, 170 bar, expansion ratio of 3.

For brevity, a full description of the model is not presented here, but can instead be found in Appendix A. Instead, a brief overview of the process is provided here. The process starts with the choice of the non-dimensional parameters, namely the flow coefficient (ϕ), and loading coefficient (ψ), which are defined as:

$$\phi = C_a / U, \tag{1}$$

$$\psi = \frac{2\Delta h_{os}}{U^2}, \tag{2}$$

where Δh_{os} is the enthalpy drop across the stage, U is the blade velocity and C_a is the axial velocity. Alongside these, the degree of reaction Λ and an initial estimate for the total-to-total isentropic efficiency are also specified. The values of the mass flow rate, turbine inlet temperature and pressure are taken from the cycle analysis. The selection of the dimensionless parameters is made with the aim of maximising turbine efficiency; the first two parameters, ϕ and ψ , according to typical values taken from the Smith chart [25], while the degree of reaction is assumed to be 0.5 [26]. Then, the loss coefficients are calculated using the selected loss model; where they are chosen to obtain an accurate estimation for the profile, secondary and tip clearance losses at the design operating conditions as detailed in Section 3. Following this, the design is re-iterated using the calculated loss coefficients and the estimate for the turbine efficiency is updated. Once the design geometry is obtained, the blade heights and mean diameter are calculated as a function of the area, mean velocity and rotational speed, and hence the feasibility of the design can be verified in comparison to the feasible manufacturing values for the inlet blade height and blade diameter [11].

Furthermore, pressure and centrifugal loads are examined where Ni-Cr-Co alloy (Inconel 718) is assumed for the turbine blades; it has been considered as a suitable material in the past [26]. The loads are calculated, assuming tapered blades with an average density of 8000 kg/m^3 and a maximum equivalent stress of 303 MPa, using Equations (A19) and (A20) [26,27]. The centrifugal load is calculated at the mean blade height and mean rotor area. To calculate the bending load, the number of rotor blades are defined as function of the blade pitch (s) at the mean radius (r_m):

$$n_R = 2\pi r_m / s, \tag{3}$$

The optimum pitch to chord ratio is obtained as a function of the flow angles and the chord length is obtained assuming an aspect ratio of 1 [28]. The design steps and methodology are summarised in Appendix A and in the flow chart (Figure 3).

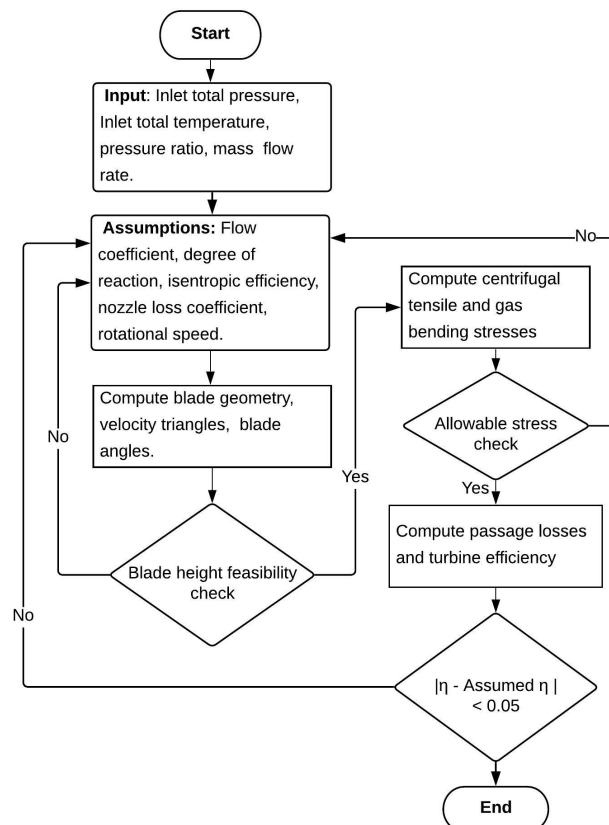


Figure 3. Design flow chart.

In principle, the optimal axial turbine efficiency occurs within a certain range of specific speed, typically $0.1 < N_s < 1.0$ [29]. For the specified specific speed range, the rotational speed ranges varies between 64 and 640 kRPM. Running the turbine at higher specific speed imposes high level of stresses on the rotor blades and could also result in rotordynamic instabilities. Consequently, in the present study the turbine design will be evaluated at three different shaft speeds, namely 150k, 200k and 250k RPM, corresponding to specific speed ranging from 0.23 to 0.39 rad, to achieve an overall turbine efficiency greater than 80%. The shaft speed is determined using Equation (4), by assuming that the specific speed is within the optimal range for axial turbines:

$$N_s = \frac{\omega \sqrt{\dot{Q}}}{\Delta h_{os}^{3/4}}, \quad (4)$$

In Equation (4), ω is the rotor rotational speed in rad/s, \dot{Q} is the volumetric flow rate at the rotor outlet in m^3/s and Δh_{os} is the isentropic enthalpy drop across the turbine, in J/kg.

To examine the effect of the various design parameters on the turbine performance and the feasibility of the design, the flow coefficient and loading coefficients have been varied over the range of 0.2 to 1 and 0.8 and 3 respectively [25]. Also, the the degree of reaction is varied from from 0–0.5 [26]. Then, the radius for root, mean, tip profiles are obtained using the free vortex design equations. Table 1 reports the range of values selected for the various design parameters.

Table 1. Input design specifications.

Design Parameter	Value	Design Parameter	Value
Turbine inlet temperature	650°C [11]	Turbine inlet pressure [MPa]	17 [22]
Expansion ratio [-]	3.0	Net power output [kW]	100
Rotational Speed [kRPM]	150–250	Flow coefficient [-]	0.2–1.0 [25]
Degree of Reaction [-]	0.0–0.5 [26]	Loading Coefficient [-]	0.8–3.0 [25]
Ni-Cr-Co density [kg/m^3]	8000	Inconel 718 equivalent stress [MPa]	303 at 1073 K [27]

3. Loss Modelling

To predict axial turbine performance, various loss models have been previously introduced starting from Soderberg [30], and then Ainley and Mathieson [31]. This has been followed by modifications presented by Dunham and Came [32], Craig and Cox [33], Kacker and Okapuu [34], and finally off-design correlations proposed by Moustapha et al. [35]. Soderberg’s loss model accounts for the effect of profile and secondary flow losses, while tip clearance and trailing edge losses are ignored. Profile losses are calculated as a function of the flow deflection while the secondary losses are interpreted as function of the aspect ratio neglecting the effect of inlet boundary layer and blade geometry. While Soderberg’s model is considered to be an oversimplified model where the effect of Mach number (Ma) and fluid non-dimensional parameters are neglected, it is considered to be satisfactory for preliminary design phase as it allows the loss within the stator and rotor to be estimated based on the amount of expansion that occurs within each passage [36]. In the presented design framework, velocities approach the sonic speed and therefore Soderberg model is considered to be more accurate for estimating the flow losses as the correlations were derived based on high Mach number data. In the absence of a tip clearance loss correlation in this model, the Ainley and Mathieson correlation has been used. It is worth mentioning that a comparative study was made between using Ainley and Mathieson correlations only and the combination of the two classes, and the same trends were observed with a deviation in the design point efficiency of approximately 1.65%. Equations (5)–(7) represent the loss coefficients predicted using Soderberg model and Equations (10)–(11) represent the tip clearance loss coefficient estimated using the Ainley and Mathieson model.

In Soderberg’s model, the losses are modelled as a function of the aspect ratio (H/l), the nominal loss coefficient ζ^* and the blade deflection ε . The nominal loss coefficient is obtained from the empirical correlation:

$$\zeta^* = 0.04 + 0.06 \left(\frac{\varepsilon}{100} \right)^2, \tag{5}$$

where ε is the flow deflection angle, which corresponds to $\varepsilon_N = \alpha_1 + \alpha_2$ for the stator and $\varepsilon_R = \beta_2 + \beta_3$ for the rotor. The nominal loss coefficients are then obtained as follows:

$$\zeta_N = \left(\frac{10^5}{Re} \right)^{1/4} \left[(1 + \zeta^*) \left(0.993 + 0.075 \frac{l}{H} \right) - 1 \right], \tag{6}$$

$$\zeta_R = \left(\frac{10^5}{Re} \right)^{1/4} \left[(1 + \zeta^*) \left(0.975 + 0.075 \frac{l}{H} \right) - 1 \right], \tag{7}$$

In Ainely and Mathieson’s model, the tip clearance coefficient Y_k is defined in terms of pressure drop as a function of the pitch to chord ratio (s/c), average blade angle β_m , the radial tip clearance (k), the average blade height (h) and a constant (B).

$$\beta_m = \tan^{-1}[(\tan \beta_3 - \tan \beta_2/2)], \tag{8}$$

$$C_L = 2 (s/c) (\tan \beta_2 + \tan \beta_3) \cos \beta_m, \tag{9}$$

where B equals to 0.5 for radial tip clearance. Considering the manufacturing tolerances and uncertainties in thermal expansion during the operation of micro-scale turbines, the radial tip clearance for the un-shrouded blades is set to 0.1 mm [6]. The tip clearance loss coefficient is then obtained as follows:

$$Y_k = B \left(\frac{k}{h} \right) \left[\frac{C_L}{s/c} \right]^2 \left[\frac{\cos^2 \beta_3}{\cos^3 \beta_m} \right], \tag{10}$$

The enthalpy loss coefficient for the rotor (λ) is then obtained as a function the rotor blade exit actual relative and isentropic temperatures ($T_{03,rel}$) and (T_3'') respectively, the rotor exit velocity (V_3) and the specific heat capacity of the working fluid (c_p).

$$\lambda_k = \frac{Y_k}{(T_{03,rel}/T_3'')} \tag{11}$$

4. Model Validation

One of the challenges that face sCO₂ turbine design is the lack of experience and published validation data available within the literature. Most of the experimental test rigs available for sCO₂ turbomachines have considered small-scale radial turbines (i.e. Sandia national laboratory (SNL), Naval nuclear laboratory (NNL), The Tokyo institute of technology (TIT), Korea atomic energy research institute (KAERI) among others) [37–40]. Furthermore, previous sCO₂ turbine designs mostly focus on large-scale turbines, for which the axial turbine is the preferred configuration. To support this study, the design model has been verified against a study conducted for a 100 MW sCO₂ axial turbine design presented by Schmitt et al. [41]. In their study, a first-row aerodynamic analysis for a six-stage 100 MW sCO₂ Brayton cycle turbine was presented. The mean-line design, integrated with Soderberg’s correlation, was implemented to predict aerodynamic losses. The results of the mean-line design were verified with a 3D simulation using STAR-CCM+; which verified the 1D mean-line design. Using the same design inputs from that study, the model developed in this work, ignoring the tip clearance losses, has been used to design the same turbine and good agreement between the two models is found (Table 2) [41]. Whilst the presented validation provides a preliminary validation for the design model, further studies (i.e., CFD and experimental) are required to ensure the suitability of the implemented

loss models for sCO₂ micro-scale axial turbines; these models were derived for air turbines and have not been validated yet for sCO₂ turbines.

Table 2. 100 kW supercritical carbon dioxide (sCO₂) turbine design model validation.

Performance Parameters	Verified [41]	Results	Difference [%]	Design Angles	Verified [41]	Results	Difference [%]
η_{tt}	0.903	0.9058	0.31	β_3	42.3	42.310	0.024
η_{ts}	0.835	0.8391	0.48	β_2	63.9	63.960	0.094
ζ_R	0.108	0.1077	0.28	α_2	70.7	70.703	0.004
ζ_N	0.070	0.0699	0.14	α_3	5.70	5.777	1.340

5. Results and Discussion

A parametric study is presented in this section to investigate the effect of the flow coefficient (ϕ), degree of reaction (Λ) and loading coefficient (ψ) on the turbine performance η_{tt} and design feasibility. Different turbine designs are generated assuming different values of the design parameters ϕ , ψ , Λ , based on the specified ranges in Table 1. Accordingly, a Smith chart is obtained as shown in Figure 4, which shows the normalised efficiency achieved for the sCO₂ turbine with a degree of reaction and rotational speed of 0.5 and 150 kRPM respectively.

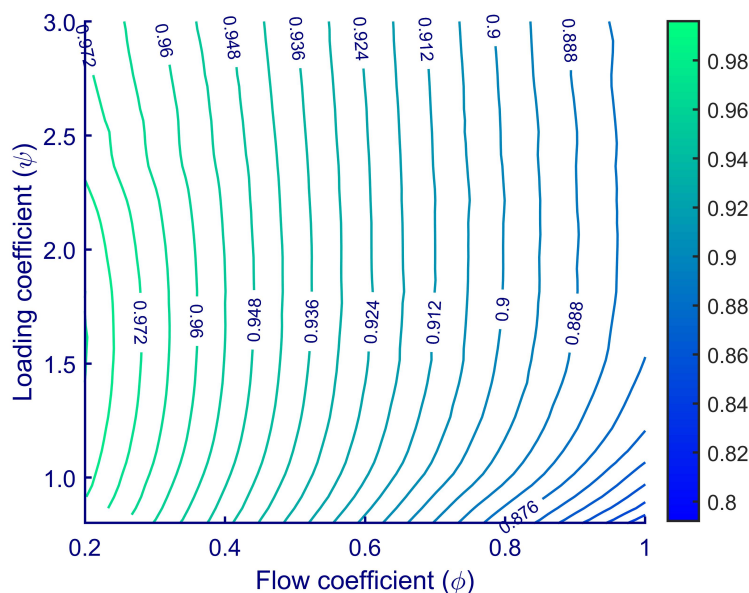


Figure 4. Contour plot for normalised sCO₂ turbine efficiency at $\Lambda = 0.5$ and 150 kRPM.

It is observed that the highest normalised efficiencies are obtained at low flow and loading coefficients, as in the original Smith chart [25]. According to Figure 4, a design point can be selected as a starting point for the parametric study. Though one of the benefits of using sCO₂ is having compact component designs, clearance losses will be proportionally larger compared to turbomachines of a comparable power rating owing to the high density of sCO₂ and small turbine dimensions. Additionally, windage losses could be expected to be significant on the turbomachinery wheel surfaces compared to large-scale gas turbines as reported from the tests conducted by the Naval Nuclear Laboratory and the Tokyo institute of technology’s (TIT) [39,40]. Therefore, whilst windage losses are not accounted for in the current study, it is important to include these in the future. Likewise, losses due to surface roughness are not considered in this analysis owing to the simplicity of the implemented loss model. Thus, the mean-line model will be extended to include both roughness and windage effects in future studies.

The effect of changing the rotor rotational speed on η_{tt} at different flow and loading coefficients has also been examined. The efficiency is found to increase linearly with increasing rotational speeds

over the range from 150 to 250 kRPM for the loading and flow coefficient domains specified in Table 1. The lowest flow coefficient, over the range from 0.2 to 1.0, results in the highest efficiency level, as confirmed in Figure 4. However, a low flow coefficient results in larger turbine annulus area and a larger deflection angle. A loading coefficient of 1.6 results in the maximum efficiency at a fixed flow coefficient and degree of reaction of 0.2 and 0.5 respectively. At a loading coefficient of 1.6, the swirl angle is kept close to the recommended value, which is recommended not to exceed 20° [26], whilst the optimum difference in the whirl velocity components at the inlet and exit of the rotor is achieved, which enables a high efficiency to be achieved. Thus, for this design, the flow coefficient and loading coefficient are set to 0.2 and 1.6 respectively to achieve the maximum efficiency at a degree of reaction of 0.5. The corresponding turbine power output is 116 kW, with a total-to-total isentropic efficiency of 78%.

In the following set of results, Figure 5a–d, ϕ and Λ have been set to 0.2 and 0.5 respectively, whilst ψ is varied from 0.8 to 3.0. Increasing the loading coefficient from 0.8 to 3.0 results in an increase in both rotor absolute and relative inlet flow angles, α_2 & β_2 , from 74 to 81° and -60 to 60° respectively as shown in Figure 5a. In principle, low loading coefficients result in higher efficiency, though it results in higher blade speed and thus high mechanical stresses; at values of 1.0 and 3.0 the mean blade speed (U_m) reaches approximately 522 and 306 m/s, and results in a total blade stresses of 160 MPa and 76 MPa respectively. Meanwhile, at high loading values a smaller number of rotor blades is needed. Therefore, the design decision should be made based on the selected material, the maximum allowable stress, along with the required number of blades.

Furthermore, increasing the loading coefficient causes a slight decrease in both Ma_2 and Ma_3 , at the inlet and outlet of the rotor blades respectively, as shown in Figure 5b; where Ma_2 and Ma_3 are the Mach numbers calculated with respect to the absolute and the relative velocity respectively. To achieve a subsonic flow at a flow coefficient of 0.2, the loading coefficient should be greater than 0.8.

Additionally, it was found that increasing the loading coefficient results in an efficiency increase until a maximum is reached at values of ψ ranging between 1.6 to 1.7 for the three rotational speeds. It's worth mentioning the ψ has a limited effect on the efficiency at all rotational speeds for a flow coefficient of 0.2. The highest efficiency is achieved for the turbine designs that keep the swirl angle α_3 close to the recommended value, which is recommended not to exceed 20° [26], along with achieving the optimum difference in the whirl velocity components at the inlet and exit of the rotor. Increasing the exit circumferential velocity, owing to the increased swirl angle, results in an increase in centrifugal force which leads to an increased amount of flow reversal at the rotor outlet. Hence, higher losses and lower efficiencies are observed.

Increasing ψ results in an increase in the blade height at the rotor inlet and outlet blade heights reaching, up to 2.1 and 3.7 mm for b_2 and b_3 respectively at a speed of 250 kRPM (Figure 5d). For feasible wheel manufacturing, it is hypothesised that inlet blade height and blade diameter should be designed to be above a minimum allowable rotor diameter of 30.00 mm and a minimum allowable blade height b_2 of 1.25 mm [11]. Thus, according to these criteria, for a design with a flow coefficient of 0.2 and rotational speed of 250 kRPM, ψ should be above 1.7. Owing to the micro-scale design dimensions, it is anticipated that micro-electrical discharge machining (EDM) milling could be used for the manufacturing of the turbine components. EDM is already in use for micro-gas turbines where high accuracy features, in the order of several micrometres, and surface finishes, with roughness values as low as $0.4 \mu m$, can be achieved [42]. Similar to this design scale, Korea institute of energy research (KIER) developed a prototype for sCO₂ Brayton cycle in which a 60 kW axial impulse turbine was manufactured; this demonstrates the ability to manufacture the turbine and the applicability of an axial turbine configuration for micro-scale applications [43].

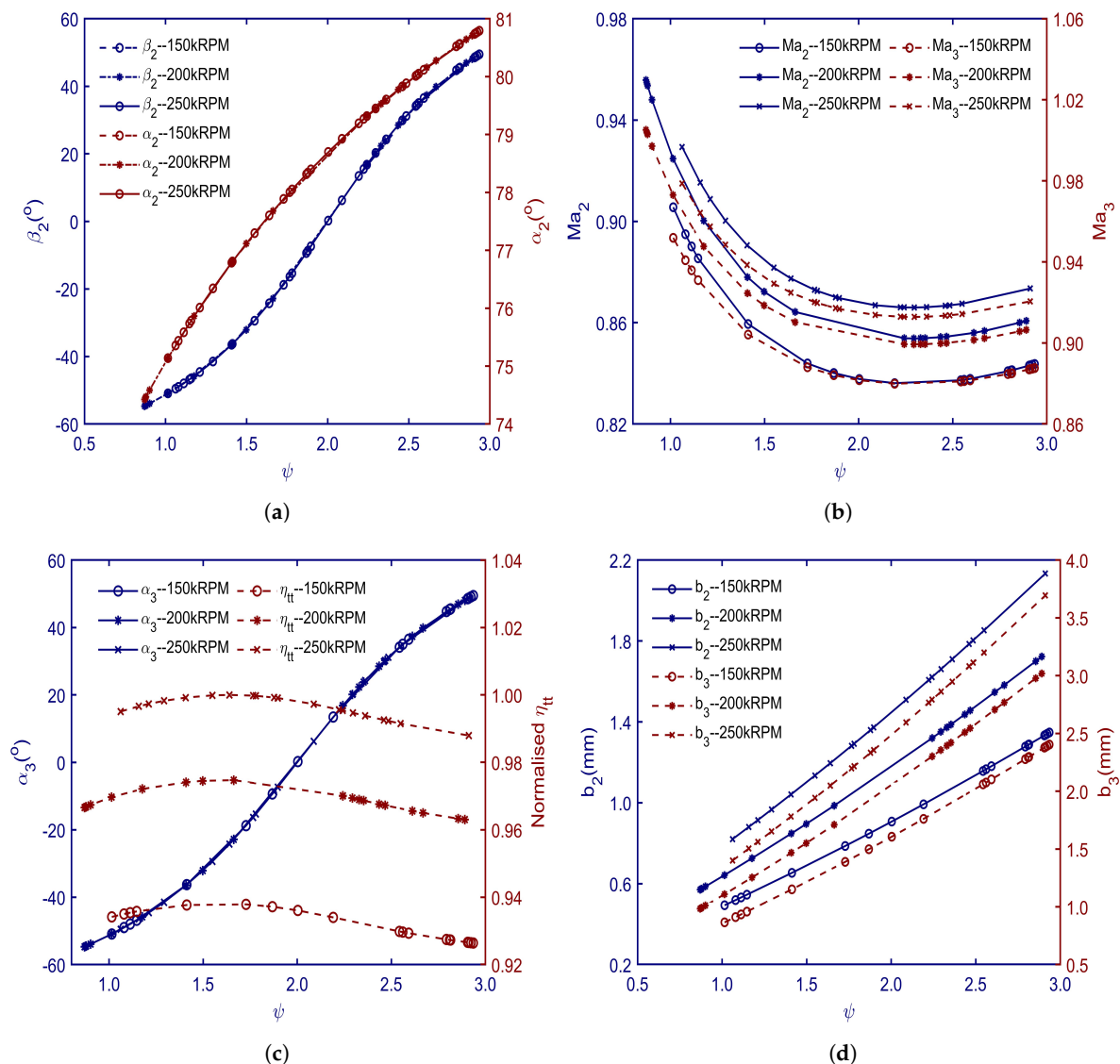


Figure 5. Loading coefficient (ψ) versus (a) flow angles [β_2 and α_2] (b) Mach number at the rotor inlet [Ma_2] and exit [Ma_3] (c) normalised efficiency [η_{tt}] and swirl angle [α_3] (d) blade heights [b_2 and b_3] at various rotational speeds.

To investigate the effect of changing the degree of reaction on the performance of the axial turbine, Λ has been varied between 0.0 and 0.5 while fixing ϕ to 0.2 and ψ to 1.6. Accordingly, the flow angle β_2 decreased from 61 to -26° and α_2 decreased from 82 to 78° as shown in Figure 6a. In the same context, increasing the degree of reaction results in an increase in Ma_3 from 0.50 to 0.92 and a decrease in Ma_2 from 1.43 to 0.90 as shown in Figure 6b. At low reaction values, the stator outlet velocity is high as a result of the large acceleration and thus the Mach number is expected to be high. A higher degree of reaction results in a thin boundary layer and less tendency to secondary flow as result of having a good acceleration at the stator outlet [44].

A noticeable decrease in the efficiency has been experienced while increasing the degree of reaction from 0.0 to 0.5, and this is found for all three of the rotational speeds considered. Particularly, the normalised efficiency decreased from 0.97 to 0.91 at a rotational speed of 150 kRPM. At high degree of reaction values, the swirl angle is small which results in less rotor losses. However, high degree of reaction results in low rotor inlet blade angles (α_2), and hence an overall reduction in the efficiency as observed in Figure 6c. In view of the fact that high reaction leads to higher pressure and high density at the rotor inlet, the blade heights decrease as the degree of reaction is increased, as shown in Figure 6d.

A maximum value of 2.20 mm was found at zero reaction and 250 kRPM and a minimum of 0.74 mm at 150 kRPM and reaction of 0.5.

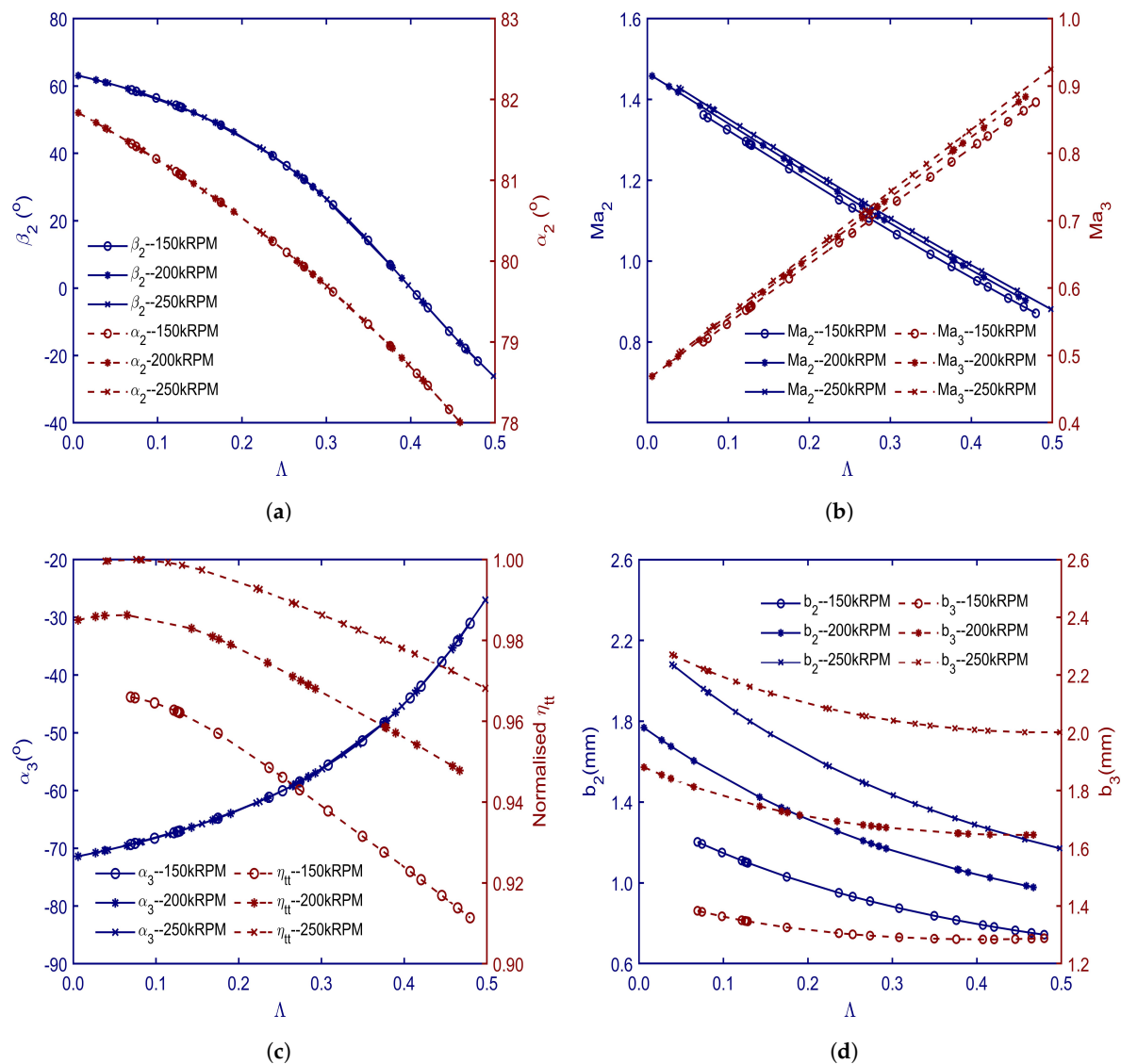


Figure 6. Degree of reaction versus (Λ) (a) flow angles [β_2 and α_2] (b) Mach number at the rotor inlet [Ma_2] and exit [Ma_3] (c) normalised efficiency [η_{tt}] and swirl angle [α_3] (d) blade heights [b_2 and b_3] at various rotational speeds.

To investigate the effect of the flow coefficient on the turbine performance, the analysis has been repeated at $\Lambda = 0.5$ and $\psi = 1.60$ respectively. Reducing ϕ over the range from 0.2 to 1 results in an increase in rotor outlet flow angle α_2 from 43 to 77° as shown in Figure 7a. However, increasing the flow coefficient also resulted in an increase in both Mach numbers, as shown in Figure 7b, where Ma_2 increased from 0.88 to 1.30 and Ma_3 increased from 0.93 to 1.34 at 250 kRPM; thus, supersonic conditions occur in both the rotor and stator. To ensure subsonic flow at the rotor inlet, the flow coefficient should be kept below 0.45 for a loading coefficient of 1.6 and degree of reaction of 0.5.

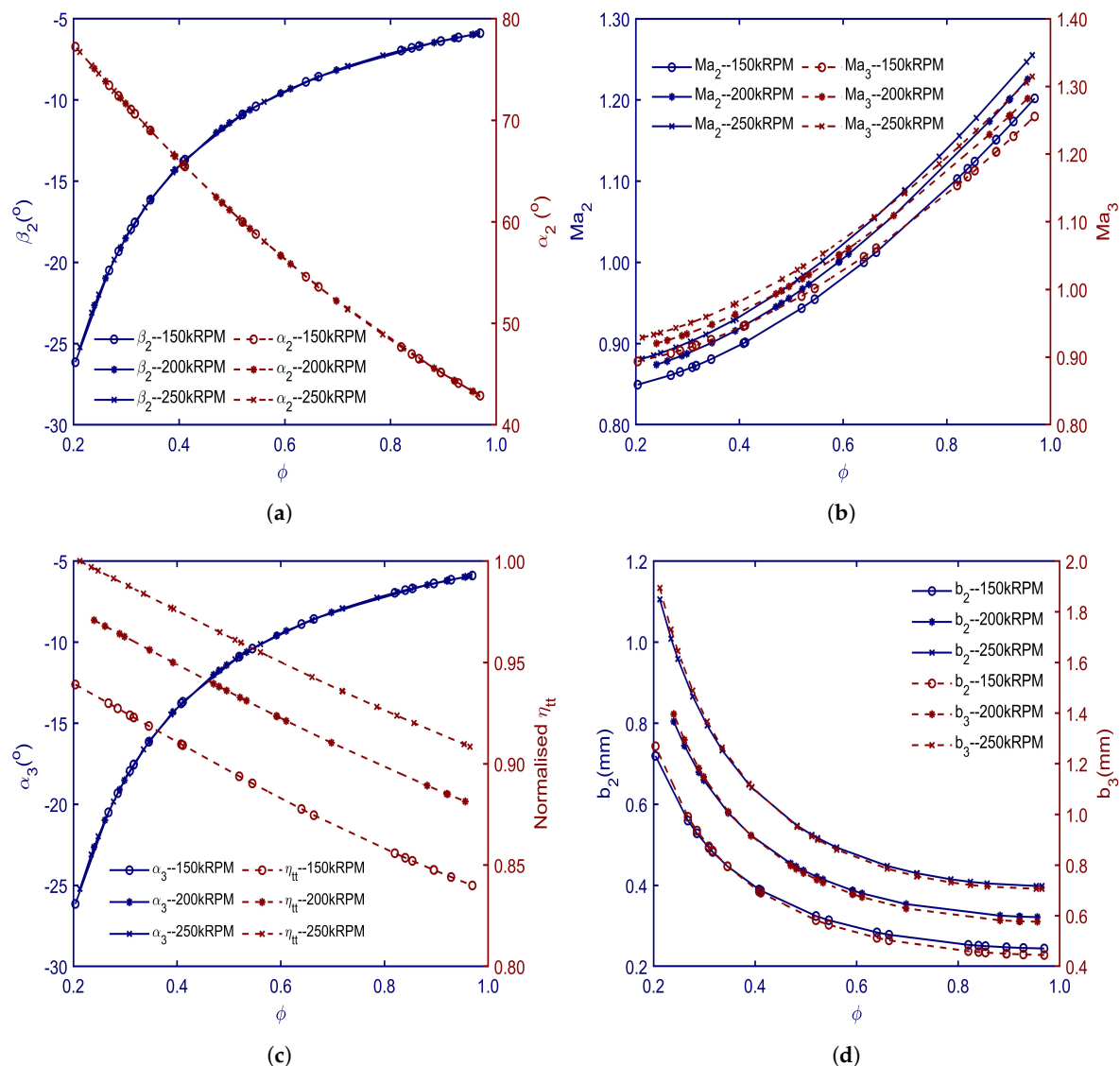


Figure 7. Flow coefficient (ϕ) versus (a) flow angles [β_2 and α_2] (b) Mach number at the rotor inlet [Ma_2] and exit [Ma_3] (c) normalised efficiency [η_{tt}] and swirl angle [α_3] (d) blade heights [b_2 and b_3] at various rotational speeds.

Furthermore, increasing the flow coefficient results in an efficiency decrease at all rotational speeds, as observed in Figure 7c. Additionally, it results in a decrease in swirl angle from 26 to 5°. However, at high flow coefficients, low swirl angles and low rotor inlet blade angles (α_2) are achieved. Increasing the flow coefficient results in higher Mach number at the rotor exit and hence higher losses incurred by the formation of shock waves in the rotor blade passages. Additionally, profile losses will be higher owing to the boundary layer growth, whilst friction losses at the exit are expected to be high. Consequently, a drop-in efficiency is observed at higher flow coefficients. The effect of changing the flow coefficient on the blade heights is shown in Figure 7d. Increasing the flow coefficient resulted in a decrease in both blade heights at all speeds. A minimum inlet blade height of 0.24 mm is found at a rotational speed of 150 kRPM and flow coefficient of 1.0.

The effect of changing the aspect ratio on the turbine efficiency is shown in Figure 8a. Increasing the aspect ratio from 1 to 3 resulted in the normalised efficiency increasing from 0.987 to 1.000 at 250 kRPM. Higher aspect ratios result in lower rotor and stator losses and higher efficiency. For high aspect ratios, secondary effects are confined to the end-wall region. However, it affects the whole passage for small aspect ratios [44]. The gas bending and centrifugal tensile stresses have been

evaluated for the selected material at a design condition of $\phi = 0.2$, $\psi = 1.6$, $\Lambda = 0.5$, 150 kRPM and aspect ratio of 1. At this point, the gas bending and centrifugal tensile stresses are predicted to be 122 and 35 MPa respectively; resulting into a total stress of 157 MPa, which falls within the material allowable limit ($\sigma_{max} = 303$ MPa). A creep failure criterion, which shows the continuous application of a steady stress over a period of time at various temperatures required to produce 0.2 percent strain, is used to assess blade life. Based on the results from [26], it is anticipated that a blade life of 10,000 hr can be achieved under these operating conditions. It is worth emphasising that creep failure is an important consideration, but a detailed analysis is outside the scope of this study.

A noticeable difference between the magnitude of the gas bending (GB) stress in comparison to the centrifugal tensile (CT) stress, for tapered blades, is experienced owing to the density effect of sCO_2 . Increasing the aspect ratio from 1 to 3 results in an increase in the gas bending stress by a factor of approximately 9. Furthermore, decreasing the degree of reaction from 0.5 to zero results in a decrease in the the gas bending stress by a factor of approximately 4. Hence, the aspect ratio and the degree of reaction should be minimised. However, decreasing the aspect ratio is associated with a drop in efficiency. Therefore, selecting the optimal aspect ratio is a trade-off between high efficiency and low stresses. Increasing the rotational speed from 150 to 250 kRPM results in centrifugal tensile stress increasing from 35 to 95 MPa as shown in Figure 8b.

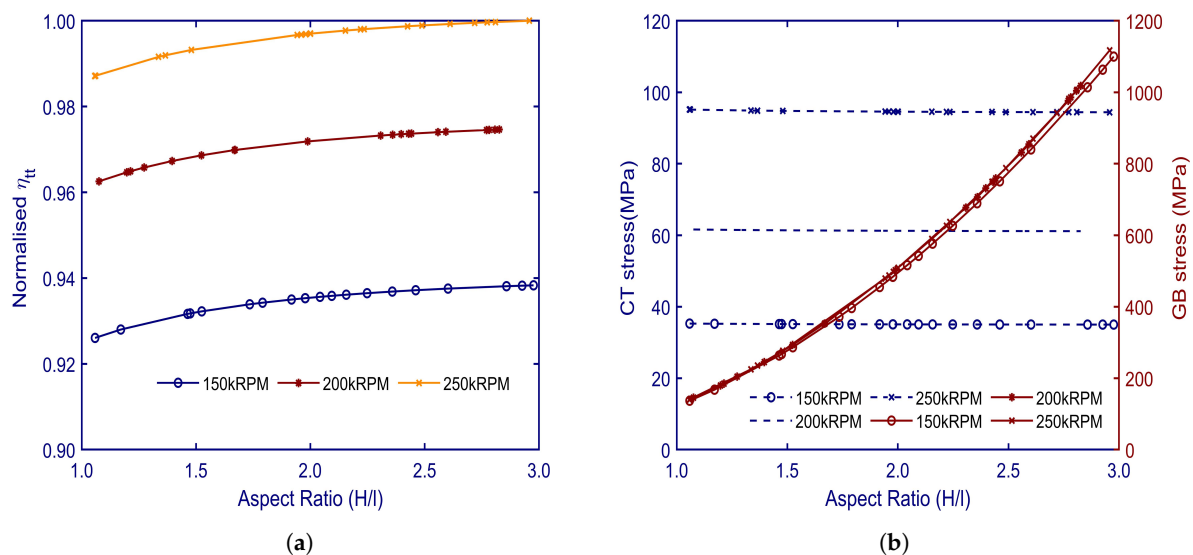


Figure 8. Aspect ratio of the rotor blades versus (a) normalised efficiency [η_{tt}] (b) centrifugal tensile [CT] and gas bending [GB] stresses at various rotational speeds.

The last part of the parametric study aims to show how the turbine design parameters can be varied to obtain a feasible turbine geometry, defined by a minimum allowable rotor diameter and inlet blade height of 30.00 mm and 1.25 mm respectively, over the range of the rotational speeds from 150 to 250 kRPM. The feasibility criteria can be achieved by operating at a high loading coefficient, where the diameter and inlet blade height are largest. Increasing the rotational speed results in a decrease in the diameter and an increase in the blade height. Hence, this should be considered during the selection of the rotational speed and flow coefficient of the turbine as shown in Figure 9a,b. The results reported in Figure 9a refer to 0.5 degree of reaction, while those in Figure 9b refer to zero degree of reaction. Thus, it can be concluded that running at a zero reaction (impulse) results in a more feasible range of inlet blade heights and diameters. The maximum diameter that can be achieved is 56 mm with a maximum inlet blade height of 3.3 mm at a flow coefficient of 0.2.

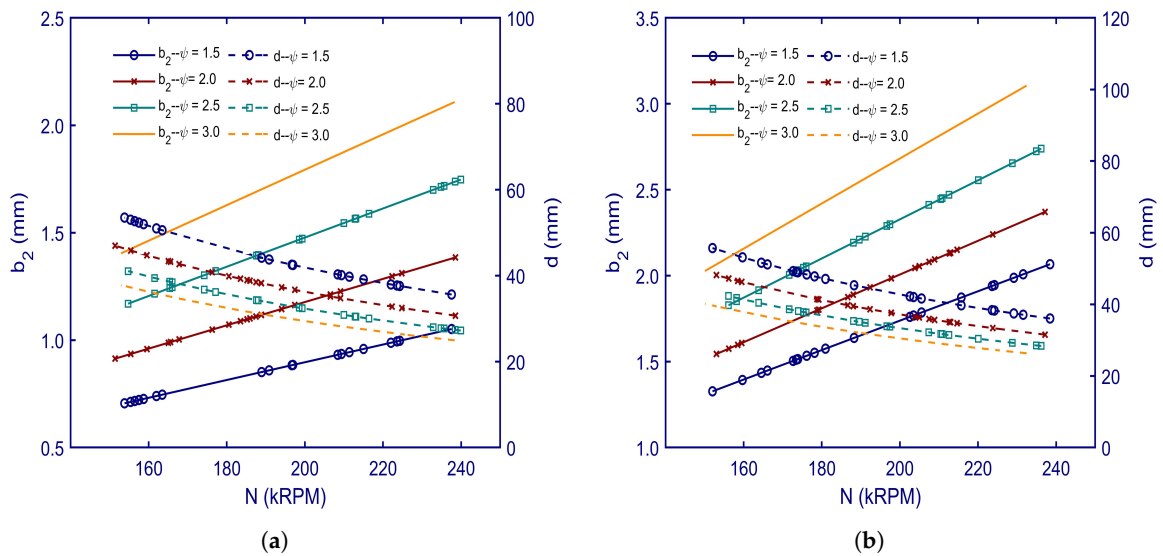


Figure 9. Rotor rotational speed versus the inlet blade height and mean diameter at (a) 0.5 degree of reaction (b) zero degree of reaction; blade height [b_2] is represented by the solid lines and diameter [d] is represented by the dashed lines.

A comparison between two turbine designs, to depict the effect of the selected design variables on the final turbine geometry, is presented in Figure 10. Geometry (A) is obtained at $\Lambda = 0.5$, $\psi = 1.6$ and $\phi = 0.2$, while geometry (B) is obtained at $\Lambda = 0.0$, $\psi = 3.0$ and $\phi = 0.2$ at 150 kRPM. Reducing the degree of reaction and increasing the loading coefficient results in more feasible design dimensions (Design B).

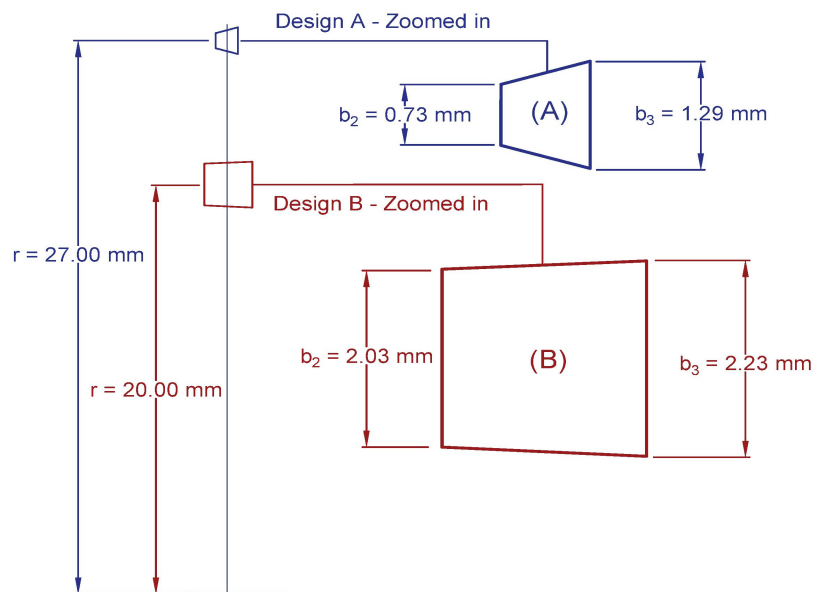


Figure 10. Comparison between two turbine designs at: (A) $\psi = 1.6$, $\phi = 0.2$ and $\Lambda = 0.5$; and (B) $\psi = 3.0$, $\phi = 0.2$ and $\Lambda = 0.0$.

6. Conclusions

This paper has presented the design of a small-scale single-stage 100 kW axial turbine for implementation within a supercritical carbon dioxide power system. The performance of the turbine was evaluated by introducing Soderberg’s and Ainley and Mathieson’s loss correlations in the design model. To verify the developed model, it was cross checked with published results for a larger turbine

design which gave confidence in the methodology. A parametric study was conducted to investigate the effects of the degree of reaction, flow coefficient and loading coefficient on the performance and the feasibility of the proposed design. The designs were assessed at three rotational speeds, namely 150, 200 and 250 kRPM, with specific speed ranging between 0.23 to 0.39 rad. It is found that feasible designs could be obtained, considering the minimum allowable inlet blade height and mean diameter, at a low flow coefficient (in the range of 0.2), a high loading coefficient (>2.8), and a low degree of reaction at a rotational speed of 150 kRPM. Additionally, low degree of reaction results in higher efficiencies owing to the high rotor inlet blade angles. High aspect ratios were found to result in high efficiencies and high stresses, and hence the selection of the optimum aspect ratio is a trade-off between the high efficiency and low stresses.

This work has demonstrated the suitability of Soderberg's and Ainley and Mathieson's models loss correlations to investigate the design of a single-stage axial turbine for sCO₂ applications. It has also provided important insights into the trade-offs between aerodynamic and mechanical design that should be considered at this scale. However, the next necessary steps would be to conduct a more detailed structural analysis, alongside extending the mean-line model to include more sophisticated loss models, and conducting 3D CFD simulations to further validate the model.

Author Contributions: All the named authors designed the presented study, A.I.S and M.T.W. provided the paper conceptualization. The Methodology was conducted by S.I.S. The software was developed by S.I.S and M.T.W. S.I.S conducted the validation, formal analysis and investigation. S.I.S and M.A.K prepared the initial manuscript and M.T.W and A.I.S reviewed and edited the paper before submission. This work has been completed under the supervision of A.I.S. and M.T.W. All authors have read and agreed to the published version of the manuscript.

Funding: The SCARABEUS project has received funding from the European Union's Horizon 2020 research and innovation programme under grant agreement No. 814985.

Conflicts of Interest: The authors declare no conflict of interest.

Abbreviations

The following abbreviations are used in this manuscript:

A	Mean blade area [m ²]
b_2	Rotor inlet blade height [mm]
b_3	Rotor exit blade height [mm]
CSP	Concentrated-solar power
CT stress	Centrifugal tensile stress [MPa]
c	Blade chord length [mm]
C	Absolute Velocity [m/s]
C_a	Axial velocity component
d	Mean blade diameter [mm]
GB stress	Gas bending stress [MPa]
h	Mean blade height [mm]
KIER	Korea institute of energy research
KAERI	Korea atomic energy research institute
\dot{m}	Mass flow rate [kg/s]
Ma	Mach number [-]
EDM	micro-electrical discharge machining
n_R	The number of rotor blades [-]
N_s	Specific speed [rad]
N	Rotational speed [kRPM]
NNL	Naval Nuclear Laboratory
\dot{Q}	Volume flow rate [m ³ /s]
r_m	Mean blade radius [mm]
RANS	Reynolds-averaged Navier–Stokes equations
RPM	Revolutions per minutes
sCO ₂	Supercritical carbon dioxide.
SNL	Sandia national laboratory

TIT	The Tokyo institute of technology
U_m	Rotor blade mean velocity [m/s]
U	Blade velocity [m/s]
V	Relative Velocity [m/s]
s	Blade pitch [mm]
α	Absolute flow angle [°]
β	Relative flow angle [°]
Δh_{os}	Enthalpy drop across the stage [kJ/kg]
Δh_o	Enthalpy drop across the entire turbine [kJ/kg]
ζ	Enthalpy loss coefficient [-]
η_{tt}	Total to total Efficiency [%]
η_{ts}	Total to static Efficiency [%]
λ	Enthalpy loss coefficient [-]
Λ	Degree of reaction [-]
ρ_b	Density of blade material [kg/m ³]
ψ	Blade loading coefficient [-]
ϕ	Flow coefficient [-]

Appendix A. Design Steps

From the thermodynamic specification of the turbine and an assumed turbine efficiency the enthalpy drop across the entire turbine Δh_o can be readily found. The blade speed U and axial velocity component C_a then follow from the loading coefficient ψ and flow coefficient ϕ :

$$U = \sqrt{\frac{2\Delta h_{os}}{\psi}} \quad (\text{A1})$$

$$C_a = U\phi \quad (\text{A2})$$

The blade angles for the stator and rotor are determined as a function of the blade speed U , the loading coefficient ψ , flow coefficient ϕ and degree of reaction Λ :

$$\tan \beta_2 = \frac{1}{2\phi} \left(\frac{\psi}{2} - 2\Lambda \right) \quad (\text{A3})$$

$$\tan \alpha_2 = \tan \beta_2 + \frac{1}{\phi} \quad (\text{A4})$$

$$\tan \beta_3 = \frac{1}{2\phi} \left(\frac{\psi}{2} + 2\Lambda \right) \quad (\text{A5})$$

$$\tan \alpha_3 = \tan \beta_3 - \frac{1}{\phi} \quad (\text{A6})$$

From the calculated angles, the absolute and relative velocities can be found and thus the thermodynamic properties at the inlet and outlet of each stage can be determined.

$$C_2 = \frac{C_a}{\cos \alpha_2} \quad (\text{A7})$$

$$C_3 = \frac{C_a}{\cos \alpha_3} \quad (\text{A8})$$

$$V_2 = \frac{C_a}{\cos \beta_2} \quad (\text{A9})$$

$$V_3 = \frac{C_a}{\cos \beta_3} \quad (\text{A10})$$

Following from an initial estimate for nozzle loss coefficient the isentropic enthalpy (h'_2) can be calculated:

$$h'_2 = h_2 - \left[\frac{1}{2} \lambda_N C_2^2 \right] \quad (\text{A11})$$

where 1, 2 and 3 subscripts correspond to stator inlet, rotor inlet and rotor exit conditions respectively.

Using the axial velocity, the area required to pass the specified mass-flow rate can be found. The passage area of the nozzle and rotor at different planes can be obtained as a function of the density ρ and axial velocity component.

$$A = \frac{\dot{m}}{\rho C_a} \quad (\text{A12})$$

The blade height b and mean radius r_m can be calculated using the blade speed and rotational speed N :

$$r_m = \frac{U}{2\pi N} \quad (\text{A13})$$

$$b = \frac{AN}{U} \quad (\text{A14})$$

The stator and rotor passage losses can be obtained using the enthalpy loss coefficients. These coefficients are expressed as a function of the enthalpy difference between an isentropic and real expansion and the kinetic energy of the flow.

$$\lambda_N = \frac{h_2 - h'_2}{C^2/2} \quad (\text{A15})$$

$$\lambda_R = \frac{h_3 - h_3''}{V^3/2} \quad (\text{A16})$$

$$W = h_{03} - h_{01} \quad (\text{A17})$$

From the estimated loss coefficients, the total-to-total isentropic efficiency can be determined.

$$\eta_{tt} = \left[1 + \left(\frac{\lambda_R \frac{V^3}{2} + \frac{C^2}{2} \lambda_N \frac{T_3}{T_2}}{h_{01} - h_{03}} \right) \right]^{-1} \quad (\text{A18})$$

Following the above blade calculations, detailed dimensions for the rotor radius at the hub and tip can be obtained by applying the free vortex theory. Additionally, the number blades and blade profile can be obtained through estimating the optimum pitch to chord ratio and pitch to throat ratio as a function of the blade angles [28].

To check the design consistency with the permissible level of stress within the rotor blades the centrifugal stress applied on the blade and the gas bending stress can be calculated using the following equations assuming a tapered blade shape:

$$\sigma_{max} = \frac{4}{3} \pi N^2 \rho_b A \quad (\text{A19})$$

$$\sigma_{bending} = \frac{\dot{m} C a [\tan \alpha_2 + \tan \alpha_3]}{n_R} \times \frac{h}{2} \times \frac{1}{z c^3} \quad (\text{A20})$$

where ρ_b is the density of blade material, n_R is the number of rotor blades, h is the mean blade height, A is the mean blade area and z is a constant obtained from a graph by Ainley [26].

References

1. Aichmayer, L.; Spelling, J.; Laumert, B. Thermo-economic Analysis of a Solar Dish Micro Gas-turbine Combined-cycle Power Plant. *Energy Procedia* **2015**, *69*, 1089–1099. [CrossRef]
2. Yin, J.; Zheng, Q.; Peng, Z.; Zhang, X. Review of supercritical CO₂ power cycles integrated with CSP. *Int. J. Energy Res.* **2019**. [CrossRef]
3. Saeed, M.; Kim, K.H. Analysis of a recompression supercritical carbon dioxide power cycle with an integrated turbine design/optimization algorithm. *Energy* **2018**, *165*, 93–111. [CrossRef]
4. Moroz, L.; Frolov, B.; Burlaka, M.; Guriev, O. Turbomachinery Flow path Design and Performance Analysis for Supercritical CO₂. In Proceedings of the ASME Turbo Expo 2014, Düsseldorf, Germany, 16–20 June 2014. [CrossRef]
5. Holaind, N.; Bianchi, G.; De Miol, M.; Saravi, S.; Tassou, S.; Leroux, R.; Jouhara, H. Design of radial turbomachinery for supercritical CO₂ systems using theoretical and numerical CFD methodologies. *Energy Procedia* **2017**, *123*, 313–320. [CrossRef]
6. Qi, J.; Reddell, T.; Qin, K.; Hooman, K.; Jahn, I. Supercritical CO₂ Radial Turbine Design Performance as a Function of Turbine Size Parameters. *J. Turbomach.* **2017**, *139*. [CrossRef]
7. Zhou, A.; Song, J.; Li, X.; Ren, X.; Gu, C. Aerodynamic design and numerical analysis of a radial inflow turbine for the supercritical carbon dioxide Brayton cycle. *Appl. Energy* **2017**, *205*, 187–209. [CrossRef]
8. Zhang, D.; Wang, Y.; Xie, Y. Investigation into Off-Design Performance of a sCO₂ Turbine Based on Concentrated Solar Power. *Energies* **2018**, *11*, 3014. [CrossRef]
9. Lv, G.; Yang, J.; Shao, W.; Wang, X. Aerodynamic design optimization of radial-inflow turbine in supercritical CO₂ cycles using a one-dimensional model. *Energy Convers. Manag.* **2018**, *165*, 827–839. [CrossRef]
10. Shi, D.; Zhang, L.; Xie, Y.; Zhang, D. Aerodynamic Design and Off-design Performance Analysis of a Multi-Stage S-CO₂ Axial Turbine Based on Solar Power Generation System. *Appl. Sci.* **2019**, *9*, 714. [CrossRef]
11. White, M.T.; Sayma, A.I. A Preliminary Comparison of Different Turbine Architectures for A 100 Kw Supercritical CO₂ Rankine Cycle Turbine. In Proceedings of the 6th International Supercritical CO₂ Power Cycles Symposium, Pittsburgh, PA, USA, 27–29 March 2018.
12. Fiaschi, D.; Manfrida, G.; Maraschiello, F. Organic Rankine Cycles, ORC turbo expander design, Combined heat and power. *Appl. Energy* **2012**, *97*, 601–608. [CrossRef]
13. Casati, E.; Vitale, S.; Pini, M.; Persico, G.; Colonna, P. Centrifugal Turbines for Mini-Organic Rankine Cycle Power Systems. *J. Eng. Gas Turbines Power* **2014**, *136*. [CrossRef]
14. Rahbar, K.; Mahmoud, S.; Al-Dadah, R.; Nima, M. Parametric Analysis and Optimization of a Small-Scale Radial Turbine for Organic Rankine Cycle. *Energy* **2015**, *83*, 696–711. [CrossRef]
15. Da Lio, L.; Manente, G.; Lazzaretto, N. DA mean-line model to predict the design efficiency of radial inflow turbines in organic Rankine cycle (ORC) systems. *Appl. Therm. Eng.* **2018**, *132*, 245–255. [CrossRef]
16. Angelino, G. Carbon Dioxide Condensation Cycles For Power Production. *J. Eng. Power* **1968**, *90*, 287–295. [CrossRef]
17. Feher, E.G. The supercritical thermodynamic power cycle. *Energy Convers.* **1968**, *8*, 85–90. [CrossRef]
18. Valencia-Chapi, R.; Coco-Enríquez, R.; Muñoz-Antón, J. Supercritical CO₂ Mixtures for Advanced Brayton Power Cycles in Line-Focusing Solar Power Plants. *Appl. Sci.* **2020**, *10*, 55. [CrossRef]
19. Binotti, M.; Invernizzi, C.; Iora, P.; Manzolini, G.; Dinitrogen tetroxide and carbon dioxide mixtures as working fluids in solar tower plants. *Sol. Energy* **2019**, *181*, 203–213. [CrossRef]
20. Manzolini, G.; Invernizzi, C.; Iora, P.; Binotti, M.; Bonalumi, D. CO₂ mixtures as innovative working fluid in power cycles applied to solar plants. Techno-economic assessment. *Sol. Energy* **2019**, *181*, 530–544. [CrossRef]
21. SCARABEUS Project Home Page. Available online: <http://www.scarabeusproject.eu/> (accessed on 26 November 2015).
22. Spadacini, C.; Pesatori, E.; Centemeri, L.; Lazzarin, N.; Macchi, R.; Sanvito, M. Optimized Cycle and Turbomachinery Configuration for an Intercooled, Recompression sCO₂ Cycle. In Proceedings of the 6th International Supercritical CO₂ Power Cycles Symposium, Pittsburgh, PA, USA, 27–29 March 2018.
23. Lemmon, E.W.; Huber, M.L.; McLinden, M.O. IST Standard Reference Database 23: Reference Fluid Thermodynamic and Transport Properties-REFPROP, Version 9.1. In Proceedings of the 6th National Institute of Standards and Technology, Standard Reference Data Program, Gaithersburg, MD, USA, 15–17 May 2013.

24. Simulis Thermodynamics. Available online: <http://www.prosim.net/en/software-simulis-thermodynamics-mixture-properties-and-fluid-phase-equilibria-calculations-3.php> (accessed on 13 November 2019).
25. Smith, S.F. A Simple Correlation of Turbine Efficiency. *J. R. Aeronaut. Soc.* **1965**, *69*, 467–470. [[CrossRef](#)]
26. Saravanamuttoo, H.; Rogers, G.; Cohen, H. Chapter 7—Axial and radial flow turbines. In *Gas Turbine Theory*, 5th ed.; Saravanamuttoo, H., Rogers, G., Cohen, H., Eds.; Pearson Education limited: Harlow, UK, 2001; pp. 305–366, ISBN 013015847X, 9780130158475.
27. Nanaware, A.; Pawar, S.; Ramachandran, M. Mechanical Characterization of Nickel Alloys on Turbine Blades. *REST J. Emerg. Trends Model. Manuf.* **2015**, *1*, 15–19.
28. Aungier, R.; Hal, C.A. Chapter 6—Preliminary Aerodynamic Design of Axial-Flow Turbine Stages. In *Turbine Aerodynamics: Axial-Flow and Radial-Flow Turbine Design and Analysis*; ASME Press: New York, NY, USA, 2005; pp. 133–165, ISBN 0791802418.
29. Dixon, S.L.; Hal, C.A. Chapter 4—Axial-Flow Turbines: Mean-Line Analysis and Design. In *Fluid Mechanics and Thermodynamics of Turbomachinery*, 5th ed.; Dixon, S.L.; Hal, C.A., Eds.; Butterworth-Heinemann: Boston, MA, USA, 2010; pp. 97–141, ISBN 978-1-85617-793-1.
30. Soderberg, C.R. *Unpublished Notes*; (quoted in reference [Dixon, 1989]); Gas Turbine Laboratory, Massachusetts Institute of Technolog: Cambridge, MA, USA, 1949.
31. Ainley, D.G.; Mathieson, G.C.R. *A Method of Performance Estimation for Axial-Flow Turbines*; H.M. Stationery Office: Richmond, UK, 1951.
32. Dunham, J.; Came, P.M. Improvements to the Ainley-Mathieson Method of Turbine Performance Prediction. *J. Eng. Power* **1970**, *92*, 252–256. [[CrossRef](#)]
33. Craig, H.R.M.; Cox, H.J.A. Performance Estimation of Axial Flow Turbines. *Proc. Inst. Mech. Eng.* **1970**, *185*, 407–424. PROC-1970-185-048-02. [[CrossRef](#)]
34. Kacker, S.C.; Okapuu, U. A Mean Line Prediction Method for Axial Flow Turbine Efficiency. *J. Eng. Power* **1982**, *104*, 111–119. [[CrossRef](#)]
35. Moustapha, S.H.; Kacker, S.C.; Tremblay, B. An Improved Incidence Losses Prediction Method for Turbine Airfoils. *J. Turbomach.* **1990**, *112*, 267–276. [[CrossRef](#)]
36. Horlock, J.H. Losses and efficiencies in axial-flow turbines. *Int. J. Mech. Sci.* **1960**, *2*, 48–75. [[CrossRef](#)]
37. Ahn, Y.; Bae, S.; Kim, M.; Cho, S.; Baik, S.; Lee, J.; Cha, J. Review of supercritical CO₂ power cycle technology and current status of research and development. *Nucl. Eng. Technol.* **2015**, *47*, 647–661. [[CrossRef](#)]
38. Wright, S.; Radel, R.; Vernon, M.; Rochau, G.; Pickard, P. *Operation and Analysis of a Super-Critical CO₂ Brayton Cycle*; Sandia Report SAND2010-0171; Sandia National Laboratories Albuquerque, NM, USA, 2010. [[CrossRef](#)]
39. Clementoni, E.; Cox, T.; King, M. Off-Nominal Component Performance in a Supercritical Carbon Dioxide Brayton Cycle. *J. Eng. Gas Turbines Power* **2015**, *138*. [[CrossRef](#)]
40. Utamura, M.; Hasuike, H.; Ogawa, K.; Yamamoto, T.; Fukushima, T.; Watanabe, T.; Himeno, T. Demonstration of Supercritical CO₂ Closed Regenerative Brayton Cycle in a Bench Scale Experiment. In *Turbo Expo: Power for Land, Sea, and Air*; American Society of Mechanical Engineers: New York, NY, USA, 2012.
41. Schmitt, J.; Willis, R.; Amos, D.; Kapat, J.; Custer, C. Study of a Supercritical CO₂ Turbine with TIT of 1350 K for Brayton Cycle With 100 MW Class Output: Aerodynamic Analysis of Stage 1 Vane. In *Turbo Expo: Power for Land, Sea, and Air*; American Society of Mechanical Engineers: New York, NY, USA, 2014; Volume 3. [[CrossRef](#)]
42. Liu, K.; Lauwers, B.; Reynaerts, D. Process capabilities of Micro-EDM and its applications. *Int. J. Adv. Manuf. Technol.* **2007**, *47*, 11–19 doi:10.1007/s00170-009-2056-1. [[CrossRef](#)]

43. Cho, J.; Shin, H.; Ra, H.; and Lee, G.; Roh, C.; Lee, B.; Baik, Y. Development of the Supercritical Carbon Dioxide Power Cycle Experimental Loop in KIER. In Proceedings of the ASME Turbo Expo 2016, Seoul, Korea, 13–17 June 2016.
44. Moustapha, H.; Zelesky, M.F.; Balnes, N.C.; Japikse, D. Chapter 3—Preliminary and through flow design. In *Axial and Radial Turbines*; Concepts NREC: White River Junction, VT, USA, 2003; pp. 65–95, ISBN 978-0933283121.



© 2020 by the authors. Licensee MDPI, Basel, Switzerland. This article is an open access article distributed under the terms and conditions of the Creative Commons Attribution (CC BY) license (<http://creativecommons.org/licenses/by/4.0/>).